Immune Netw. 2025 Feb;25(1):e9
https://doi.org/10.4110/in.2025.25.e9
pISSN 1598-2629·eISSN 2092-6685

IMMUNE NETWORK

Original Article



# Mitochondrial Regulator CRIF1 Plays a Critical Role in the Development and Homeostasis of Alveolar Macrophages via Maintaining Metabolic Fitness

**Ein Lee** [1,†], **Seung Geun Song** [1,2,†], **Haaun Moon** [1], **Minho Shong** [3], **Doo Hyun Chung** [1,2,*]

[1]Laboratory of Immune Regulation, Department of Biomedical Sciences, Seoul National University College of Medicine, Seoul 03080, Korea
[2]Department of Pathology, Seoul National University College of Medicine, Seoul 03080, Korea
[3]Graduate School of Medical Science and Engineering, Korean Advanced Institute of Science and Technology (KAIST), Daejeon 34141, Korea



**Received:** Nov 28, 2024
**Revised:** Jan 13, 2025
**Accepted:** Jan 20, 2025
**Published online:** Feb 14, 2025

***Correspondence to**
**Doo Hyun Chung**
Department of Pathology and Laboratory of Immune Regulation, Department of Biomedical Sciences, Seoul National University College of Medicine, 103 Daehak-ro, Jongno-gu, Seoul 03080, Korea.
Email: doohyun@snu.ac.kr

[†]Ein Lee and Seung Geun Song equally contributed to this work.



**ORCID iDs**
Ein Lee
https://orcid.org/0000-0002-9363-5317
Seung Geun Song
https://orcid.org/0000-0002-1605-2708
Haaun Moon
https://orcid.org/0009-0002-7905-9138
Minho Shong
https://orcid.org/0000-0002-0247-7115

## ABSTRACT

The importance of mitochondrial function in macrophages is well established. Alveolar macrophages (AMs), the tissue-resident macrophages (TRMs) of the lung, are particularly dependent on mitochondria-driven oxidative phosphorylation (OXPHOS) to support their functions and maintain homeostasis. However, the specific genes and pathways that regulate OXPHOS in AMs remain unclear. In this study, we investigated the role of CR6-interacting factor 1 (CRIF1), a mitochondrial regulator, as a key factor that specifically modulates the metabolic fitness and maintenance of AMs. Using single-cell RNA sequencing and transcriptomic analyses, we found CRIF1 to be highly expressed in AMs compared to TRMs from other tissues, correlating with enhanced OXPHOS activity. Genetic ablation of *Crif1* in macrophages resulted in a marked reduction in AM populations exclusively in the lung, while other TRM populations were unaffected. CRIF1-deficient AMs exhibited an altered metabolic profile, including impaired mitochondrial function, increased glycolysis, and aberrant lipid accumulation. These findings underscore the essential role of CRIF1 in regulating mitochondrial functions and metabolic fitness in AMs, distinguishing it from broader mitochondrial regulators like mitochondrial transcription factor A, which operates across multiple TRM populations. Our study provides critical insights into the tissue-specific regulation of macrophage metabolism and suggests potential therapeutic avenues for lung diseases associated with AM dysfunction.

**Keywords:** Alveolar macrophages; Mitochondria; Metabolic reprogramming; Homeostasis; Oxidative phosphorylation

## INTRODUCTION

Tissue-resident macrophages (TRMs) are a diverse group of phagocytes with distinct features shaped by their local environments (1). TRMs, compared to their hematopoietic stem cell-derived counterparts, predominantly utilize oxidative phosphorylation (OXPHOS) during homeostasis (2,3). Among these, alveolar macrophages (AMs) in the lung are especially known to rely heavily on OXPHOS to maintain their functions and homeostasis (4). AMs,

Doo Hyun Chung
https://orcid.org/0000-0002-9948-8485

### Conflict of Interest

The authors declare no potential conflicts of interest.

### Abbreviations

AM, alveolar macrophage; BAL, bronchoalveolar lavage; BMDM, bone marrow-derived macrophage; CRIF1, CR6-interacting factor 1; ECAR, extracellular acidification rate; GEO, Gene Expression Omnibus; GLUT1, glucose transporter 1; IM, interstitial macrophage; KEGG, Kyoto Encyclopedia of Genes and Genomes; MMP, mitochondrial membrane potential; MT-CO1, mitochondrially encoded cytochrome c oxidase I; OCR, oxygen consumption rate; OXPHOS, oxidative phosphorylation; PM, peritoneal macrophage; PPAR-γ, peroxisome proliferator-activated receptor-γ; RPM, red pulp macrophage; scRNA-seq, single-cell RNA sequencing; SDHA, succinate dehydrogenase complex flavoprotein subunit A; SSC, side-scatter; TFAM, mitochondrial transcription factor A; TRM, tissue-resident macrophage; UMAP, Uniform Manifold Approximation and Projection.

### Author Contributions

Conceptualization: Chung DH; Formal analysis: Lee E, Song SG, Moon H; Investigation: Lee E, Song SG, Moon H, Shong M; Writing - original draft preparation: Lee E, Song SG, Moon H; Writing - review & editing: Lee E, Song SG, Moon H, Shong M, Chung DH.

as sentinels of the alveolar space, effectively phagocytose pathogens and particulate matter, suppress inflammation, and are essential for maintaining lung homeostasis. Studies have highlighted the critical role of metabolic reprogramming in macrophages, suggesting that alterations in mitochondrial dynamics can significantly influence macrophage behavior and immune responses (5). Therefore, understanding metabolic dependencies of AMs provides insight into how they can be manipulated for treating various lung conditions, including infection, chronic inflammatory diseases, and cancer.

Previous research has identified mitochondrial transcription factor A (TFAM), which regulates mitochondrial DNA replication, as an essential transcription factor for AMs (4,6). TFAM deletion in macrophages results in significant reduction of TRMs including AMs, demonstrating its overarching role in TRM homeostasis (4). However, while TFAM broadly regulates mitochondrial function across different TRMs, the specific pathways required for the fitness of AMs remain unclear. Identifying the key molecular regulators in governing metabolic homeostasis can deepen our understanding of the metabolic regulation of AMs.

Our study sought to address this gap by investigating CR6-interacting factor 1 (CRIF1), a mitochondrial regulator, which appears to play a unique role in the metabolic fitness and maintenance of AMs. Among TRMs from several tissues, lung AMs were especially enriched in OXPHOS signatures. We identified CRIF1 as a highly expressed mitochondrial regulator in AMs compared to other TRM counterparts. CRIF1 was required for mitochondrial homeostasis in AMs, and ablation of CRIF1 in macrophages specifically led to drastic reduction of AM populations, but not other TRMs. CRIF1-depleted AMs exhibited impaired mitochondrial ROS production and displayed abnormal lipid accumulation. Overall, we identified an essential role for CRIF1 in regulating mitochondrial function particularly in AMs, highlighting its contribution to their cellular maintenance and functional integrity.

## MATERIALS AND METHODS

### Single-cell RNA sequencing (scRNA-seq) data analysis

Publicly deposited scRNA-seq data of murine TRMs from the heart, liver, lung, kidney, and brain were obtained from the Gene Expression Omnibus (GEO) database under the accession code GSE188647 (7). Analyses were conducted in R 4.0.5 (R Foundation for Statistical Computing, Vienna, Austria) using the Seurat package version 4.0.2 (8). Initially, TRMs from each organ were processed separately. Low-quality cells were excluded based on mitochondrial gene percentage and unique feature counts. Potential contaminating cell types, including lymphoid cells, dendritic cells, and monocytes were removed based on the expression of specific marker genes and the clustering pattern in the Uniform Manifold Approximation and Projection (UMAP) plot (7). The Seurat objects for each organ were then merged, integrated, and subjected to the standard Seurat workflow including normalization, identification of highly variable features, principal component analysis, and clustering. For AM subset analysis, cell types within each cluster were annotated based on the expression of established marker genes (*Siglecf* for mature AMs, *Itgam* for immature AM-like cells, and *Mki67* for cycling cells). To estimate the activity of metabolic pathways, the oxidative phosphorylation gene set (mmu00190) from the Kyoto Encyclopedia of Genes and Genomes (KEGG) pathway database was used and module scores were calculated with the 'AddModuleScore' function, which computes the average expression levels of a given gene set to generate an aggregate pathway activity score.

Gene Set Enrichment Analysis (GSEA) was performed using the EnrichR package version 3.2 (9). Enrichment analysis was conducted with the 'DEenrichRPlot' function from EnrichR, using the processed Seurat object for mature AMs as input. The "Hallmark_2020" and "GO_Biological_Process_2023" libraries were applied for the analysis, with a log-fold change cutoff set as >0.25. For the "Hallmark_2020" library, all statistically significant gene sets with an adjusted p-value (q-value) below 0.05 (n=18 in *Crif1*-high AMs) were visualized. For the "GO_Biological_Process_2023" library, the top 20 enriched gene sets for both *Crif1*-high and *Crif1*-low AMs were visualized. All visualizations were created using bubble plots generated from GraphPad Prism 9 (GraphPad Software Inc., San Diego, CA, USA).

## ImmGen RNA sequencing analysis

The RNA sequencing data for mononuclear phagocytes from 14 organs was downloaded from the GEO repository under accession number GSE122108 (10). Resident mononuclear phagocytes from different organs were defined based on specific markers: AMs were identified as F4/80$^+$CD11c$^+$Siglec-F$^+$, CD45$^+$Ly6G$^-$Siglec-F$^+$CD11c$^+$, and CD45$^+$CD11b$^{lo}$CD64$^+$CD11c$^+$Siglec-F$^+$ cells; microglia as CD45$^{lo}$CD11b$^+$, lin$^-$PI$^-$CD45$^{int}$CD11b$^+$ and CD19$^-$CD3$^-$Ly6G$^-$CD45$^{lo}$CD11b$^+$CD64$^+$F4/80$^{lo}$CD206$^-$ cells; Kupffer cells as Clec4F$^+$Tim4$^+$CD45$^+$F4/80$^+$CD64$^+$ cells; peritoneal macrophages (PMs) as F4/80$^+$ICAM2$^+$ cells; and red pulp macrophages (RPMs) as CD19$^-$Ly6G$^-$CD115$^-$CD45$^+$CD11b$^{lo}$F4/80$^+$MerTK$^+$CD64$^+$ and CD45$^+$CD11b$^{lo}$CD64$^+$CD11c$^+$Siglec-F$^+$ cells. Raw counts were normalized by sample age and organ using the DESeq2 R package version 1.40.2. Normalized counts were z-transformed, and the expression levels of genes involved in oxidative phosphorylation (KEGG mmu00190) were visualized using heatmaps generated with GraphPad Prism 9 (GraphPad Software Inc.).

## Mice

LysM-Cre (C57BL/6J background) transgenic mice were purchased from Jackson Laboratory (Bar Harbor, ME, USA). *Crif1*$^{fl/fl}$ mice (11), a gift from Professor M. Shong (Korea Advanced Institute of Science and Technology, Daejeon, Korea), were crossed with LysM-Cre mice to generate LysM-Cre *Crif1*$^{fl/fl}$ (*Crif1*-mKO) mice. The mice were maintained in an American Association for Accreditation of Laboratory Animal Care International accredited (accreditation certificate No. 001169), specific pathogen-free barrier facility at the Biomedical Research Institute of Seoul National University Hospital (Seoul, Korea). All animal experiments were conducted in accordance with guidelines approved by the Institutional Animal Care and Use Committee of Seoul National University Hospital. Unless otherwise indicated, mice aged 6–8 wk were used for all studies. The exact number of animals used is indicated in the figure legends.

## Generation of bone marrow-derived macrophages (BMDMs)

For the generation of BMDMs, femurs and tibias from mice were flushed with PBS and treated with RBC lysis solution while filtering through a 35 μm cell strainer. The obtained cells were cultured for 6–7 days in 10% DMEM medium (DMEM with 10% FBS, 1% penicillin and streptomycin, and 1% L-glutamine) supplemented with 40 ng/ml of recombinant murine macrophage colony-stimulating factor (rmM-CSF, 576408; BioLegend, San Diego, CA, USA). Additional rmM-CSF was added to the cells on day 3. The purity of differentiated BMDMs was measured by flow cytometry for F4/80 and CD11b expression.

## Quantitative real-time PCR

Total RNA was extracted using TRIzol reagent (TR 188; MRC Inc., Cincinnati, OH, USA). RNA samples were hybridized with oligo dT (Bionics, Seoul, Korea), and reverse-transcribed into complementary DNA using the Maloney murine leukemia virus reverse transcriptase Taq polymerase (M1705; Promega, Madison, WI, USA). Real-time PCR was performed using the CFX Connect Real-Time PCR Detection System (Bio-Rad, Hercules, CA, USA). SYBR green-based quantitative PCR was conducted according to the manufacturer's instructions with specific primers for *Crif1* (forward: CAGCCTACTAGGTGTGGCG; reverse: GTAACGCGCGAACTGCTTAG) and *Actb* (forward: ATGGATGATGATATCGCCGCGCTC; reverse: ACATAGGAATCCTTCTGACCCATGCC). Data was normalized to the expression level of the endogenous control *Actb*.

## Immunoblotting

A minimum of $1.0\times10^6$ BMDMs were homogenized in cell lysis buffer containing 20 mM Tris-HCl (pH 7.9), 120 mM NaCl, 1% Triton X-100, 2.5 mM EDTA, and 2 mM dithiothreitol, along with protease inhibitor (P3100-005; GenDEPOT, Katy, TX, USA) and phosphatase inhibitor (P3200-005; GenDEPOT). Protein concentration was determined using the Bradford assay (500-0205; Bio-Rad) according to the manufacturer's instruction. Protein extracts were loaded onto 10% SDS-PAGE gels and transferred onto a polyvinylidene fluoride membrane (IPVH00010; Millipore, Burlington, MA, USA). Membranes were blocked with 5% skim milk (232100; BD, Franklin Lakes, NJ, USA) for 1 h at room temperature, followed by incubation with primary Abs overnight at 4°C on a shaker. Membranes were incubated with secondary Abs for at least 1 h at room temperature before protein detection using the Amersham™ Imager 680 (GE Healthcare, Chicago, IL, USA). Primary Abs used include anti-β-Actin (bs-0061R, 1:2,000; Bioss, Woburn, MA, USA) and anti-CRIF1 (sc-374122, 1:1,000; Santa Cruz Biotechnology, Dallas, TX, USA).

## Seahorse real-time cell metabolic analysis

The Mito Stress Test and Glycolysis Stress Test were performed to measure oxygen consumption rate (OCR) and extracellular acidification rate (ECAR), respectively. Prior to the assay, approximately $2\times10^5$ BMDMs were seeded in a 24-well XF Cell Culture Microplate (Agilent Technologies, Santa Clara, CA, USA) in BMDM growth medium. The Sensor Cartridge (Agilent Technologies) was hydrated in Seahorse XF calibrant at 37°C in a $CO_2$-free incubator overnight. On the day of the assay, the growth medium was replaced with Seahorse XF Base Medium (Agilent Technologies) containing 2 mM L-glutamine, 1 mM sodium pyruvate, or 25 mM D-glucose depending on the assay type, followed by a 1-h incubation in a 37°C $CO_2$-free incubator. Each compound was loaded into the port of the hydrated Sensor Cartridge as required. For OCR measurement, oligomycin (1 μM), carbonyl cyanide-4-(trifluoromethoxy) phenylhydrazone (1 μM), and rotenone (1 μM)/antimycin A (1 μM) were sequentially added. For ECAR measurement, glucose (10 mM), oligomycin (1 μM), and 2-deoxy-D-glucose (50 mM) were sequentially added. Data was collected using XFe24 Extracellular Flux Analyzer (Seahorse Bioscience, Bothell, WA, USA) and analyzed with Seahorse XF software.

## Single cell suspension preparation

Mice brains and lungs were mechanically dissociated and treated with type IV collagenase (C5138; Sigma-Aldrich, St. Louis, MO, USA) in DMEM at 37°C with shaking at 200 rounds per minute for 30 min or 1 h, respectively. Following digestion, brain cells were centrifuged using a Percoll (17-0891-01; GE Healthcare) gradient, where immune cells were obtained from the 30% and 70% interfaces. Livers were minced and digested in DMEM supplemented with

10% FBS and type IV collagenase for 1 h. After digestion, cells were further dissociated by passing them through an 18-gauge needle using a syringe, followed by filtration through a 70 μm strainer. Splenocytes were prepared by grinding spleens on a mesh sieve. Peritoneal cells were collected by injecting 3 ml of collection buffer (0.5% BSA in PBS) with a syringe into the peritoneal cavity and aspirating the fluid. All prepared cells were treated with RBC lysis solution (420301; BioLegend).

## Flow cytometry and cell sorting

Lung single cells were prepared as mentioned above, washed with PBS, and incubated with Zombie Aqua Fixable Viability dye (423102; BioLegend) for 8 min at room temperature for dead cell exclusion. Anti-CD16/32 Abs (553142; BD) were then added for 10 min at 4°C to block nonspecific Fc receptor binding. For surface staining, cells were incubated with Abs in FACS buffer (0.5% BSA, 0.05% sodium azide in PBS) for 30 min at 4°C. For intracellular protein detection, cells were fixed and permeabilized using the eBioscience™ FoxP3/Transcription Factor Staining Buffer Kit (00-5123-43; Invitrogen, Waltham, MA, USA) as per the manufacturer's instructions, then stained with intracellular Abs overnight at 4°C. The list of the Abs used is as follows: Alexa Fluor 647 anti-CRIF1 (sc-374122; Santa Cruz Biotechnology); Alexa Fluor 405 anti-glucose transporter 1 (GLUT1, ab210438; Abcam, Cambridge, UK); FITC anti-mouse F4/80 (123108), PE anti-mouse F4/80 (123110), APC anti-mouse F4/80 (123116), Brilliant Violet 421 anti-mouse CD11b (101251), PerCP/Cyanine5.5 anti-mouse CD11b (101228), Alexa Fluor 700 anti-mouse CD11b (101222), APC anti-mouse CD45 (103112), Alexa Fluor 700 anti-mouse CD45 (157210), PerCP anti-mouse CD45 (103130), PE/Cyanine7 anti-mouse CD11c (117318), PE anti-mouse Siglec-F (155506), Brilliant Violet 421 anti-mouse Siglec-F (155509), PerCP anti-mouse Ly-6G (127654), all from BioLegend. Flow cytometry data were acquired using a BD LSR Fortessa/Fortessa X-20 flow cytometer (BD) and analyzed with Flowjo X 10.0.7r2 software (BD). Cell sorting was performed using a BD Aria III flow cytometer (BD). For all populations, a pre-gating strategy of singlets, viability for live cells (Zombie aqua$^-$), immune (CD45+), and size selection (FSC$^{hi}$SSC$^{hi}$) was applied, after which immune cell subsets were defined as follows: CD11b$^+$F4/80$^+$ BMDM, CD45$^{int}$CD11b$^+$ microglia, CD45$^+$F4/80$^+$CD11b$^{int}$ Kupffer cells, CD45$^+$CD11c$^+$F4/80$^+$ lung AMs, CD45$^+$CD11c$^-$F4/80$^+$ lung interstitial macrophages (IMs), CD45$^+$F4/80$^+$CD11b$^+$ PMs, CD45$^+$F4/80$^+$CD11b$^-$ splenic RPMs, CD45$^+$CD11c$^+$F4/80$^+$ bronchoalveolar lavage (BAL) fluid AMs, CD45$^+$CD11c$^+$F4/80$^+$Siglec-F$^+$CD11b$^-$ mature AMs, CD45$^+$CD11c$^+$F4/80$^+$Siglec-F$^-$CD11b$^+$ immature AMs.

## Mitochondrial assays

For the quantification of mitochondrial ROS, mitochondrial membrane potential (MMP), and mitochondrial mass, cells were stained with 5 μM MitoSOX Red (M36008; Invitrogen), 10 nM MitoTracker Orange CMTMRos (M7510; Invitrogen), and 50 nM MitoTracker Green (M7514; Thermo Fisher, Waltham, MA, USA), respectively, for 15 min at room temperature. Samples stained with MitoSOX Red or MitoTracker Orange were subsequently fixed using 4% formaldehyde solution (F0161; Samchun, Seoul, Korea) for 15 min at room temperature, and then analyzed by flow cytometry within 1 h.

The MitoBiogenesis™ Flow Cytometry Kit (ab168540; Abcam) was used to evaluate the capacity of mitochondrial biogenesis. Cells were fixed with 4% formaldehyde solution and permeabilized with pre-chilled 90% methanol for 1 h at −20°C. After surface staining, cells were blocked with 1% BSA solution in distilled water and stained with Ab cocktails for mitochondrial proteins mitochondrially encoded cytochrome c oxidase I (MT-CO1) and succinate dehydrogenase complex flavoprotein subunit A (SDHA).

Total cellular ATP was quantified using BioTracker™ ATP-Red Live Cell Dye (SCT045; Sigma-Aldrich). Cells were incubated with the dye for 15 min at room temperature followed by standard preparation for flow cytometry.

### Labeling of neutral lipids

Intracellular neutral lipid content was measured by staining cells with BODIPY™ 493/503 (D3922; Thermo Fisher) at 5 μM according to the manufacturer's instructions. Cells were then analyzed with a flow cytometer.

### Diff-Quik staining

The morphology of AMs was assessed using the Diff-Quik™ Staining Set (1-736131; RAL Diagnostics, Martillac, France) according to the manufacturer's instructions. Approximately $4\times10^4$ BAL fluid cells in 200 μL PBS were cytocentrifuged onto microscopic slides. The air-dried smears were dipped at least 5 times each in Fixation Solution, Stain Solution I, and Stain Solution II. The slides were then gently rinsed under running tap water and examined under a light microscope.

### Statistical analysis

Statistical analyses were performed using GraphPad Prism 9 (GraphPad Software Inc.). Student's t-test was used for comparisons between 2-groups.

## RESULTS

### AMs are characterized by heightened mitochondrial respiration

Given the intimate relationship between metabolic pathways and macrophage functions, we first sought to examine the metabolic profiles of TRMs. Using a public scRNA-seq dataset consisting of TRMs from the heart, liver, lung, kidney, and brain, we identified organ-dependent segregation of TRM populations based on UMAP clustering (**Fig. 1A**) (7). Pathway analysis revealed that AMs were enriched for genes related to OXPHOS, the key energy transducing process maintained by mitochondria (**Fig. 1B**, **Supplementary Fig. 1A**). We further explored the landscape of OXPHOS within AMs. Even after excluding immature and cycling cells, mature AMs exhibited significant heterogeneity in OXPHOS levels between individual cells (**Fig. 1C-E**, **Supplementary Fig. 1B-D**). To better understand this heterogeneity, next we examined the expression levels of mitochondrial biogenesis-related genes across these mature AM subclusters (12). Among these genes, *Crif1* (also known as *Gadd45gip1*) expression showed a clear correlation with OXPHOS scores across subclusters, unlike other mitochondrial regulator genes, which did not display a consistent pattern (**Fig. 1F**). AM subclusters with higher OXPHOS scores consistently exhibited high levels of *Crif1* expression, which allowed for the distinction of cells with high and low *Crif1* levels within the mature AM population (**Fig. 1F and G**). Moreover, OXPHOS levels in each subset closely aligned with *Crif1* expression in their respective clusters (**Fig. 1H**). When comparing the expression of mitochondrial biogenesis-related genes among TRMs from different organs, *Crif1* showed particularly high expression levels in the lung, along with *Mfn1*, *Tfb2m*, and *Ppargc1b* (**Supplementary Fig. 1E**). We further validated the implication of *Crif1* as an AM-specific mitochondrial regulator through the analysis of another transcriptomic dataset of TRMs across organs (10). Consistent with the scRNA-seq analysis results, the overall expression levels of OXPHOS-related genes were higher in AMs compared to TRMs in other organs, including microglia, Kupffer cells, PMs, and splenic RPMs (**Supplementary Fig. 1F**). Notably, *Crif1* was expressed

at significantly higher levels in AMs compared to other TRMs (**Fig. 1I**). Taken together, these findings underscore the importance of mitochondria-mediated OXPHOS in AMs and advocate a potential role of CRIF1 for this process. CRIF1 has been reported to be required for mitochondrial functionality in several tissue types, but its role in TRMs remains unexplored (12-14).

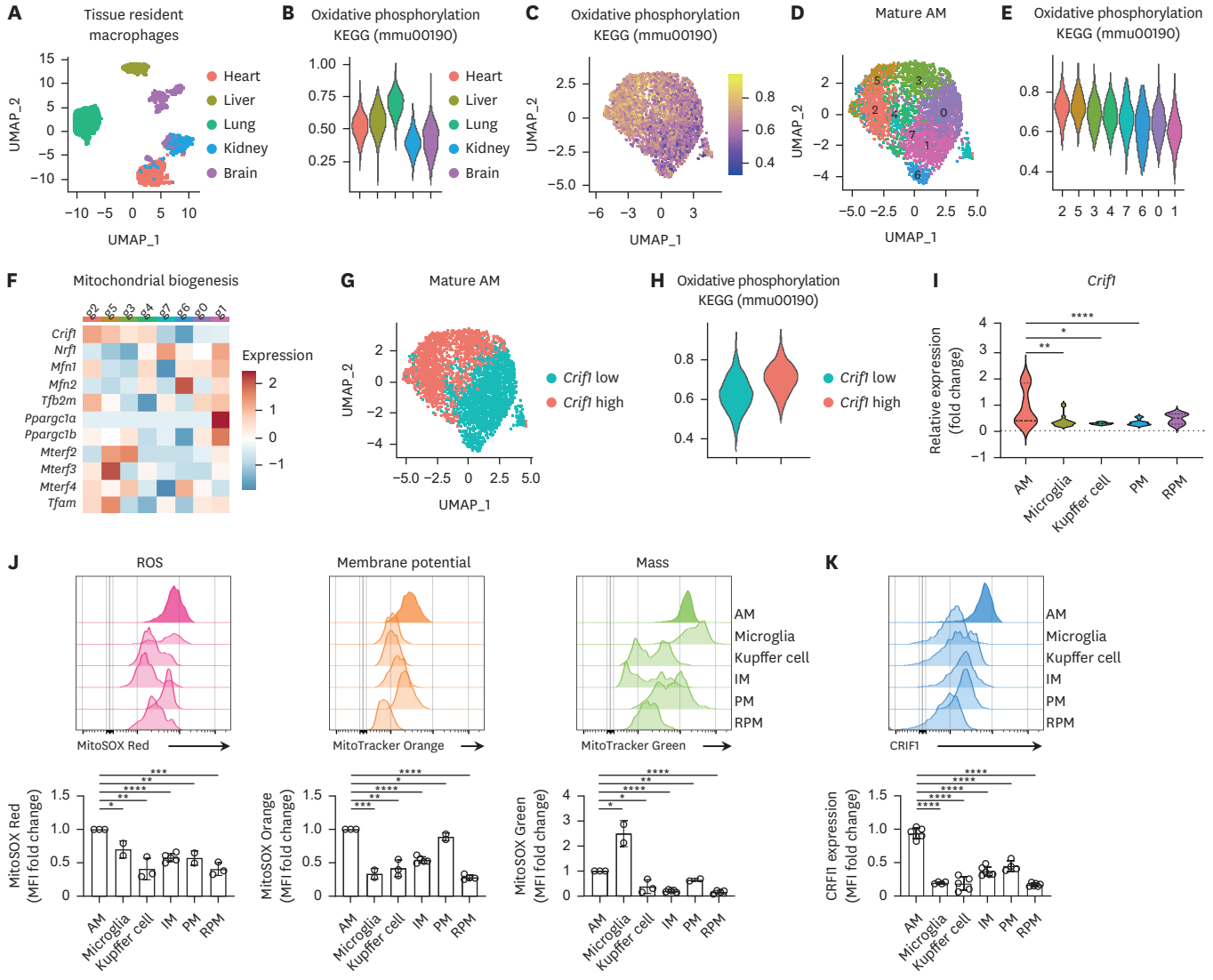


**Figure 1.** Mitochondrial OXPHOS is enhanced in alveolar macrophages.
Analysis of TRMs using scRNA-seq data from Dick et al. (7) (GSE188647). (A) UMAP visualization of TRMs from the heart (n=2,647), liver (n=1,032), lung (n=3,580), kidney (n=1,637), and brain (n=1,058). (B) Average expression levels (module scores) of OXPHOS (KEGG mmu00190) genes across TRM subsets, calculated using the AddModuleScore function in Seurat. (C) Scatter plot showing the heterogeneity of OXPHOS module scores among mature AM cells (n=3,393). (D) UMAP visualization of mature AMs, divided into 8 subclusters. (E) Average OXPHOS module scores across mature AM subclusters, ordered by decreasing score levels. (F) Expression levels of mitochondrial biogenesis-related genes across mature AM subclusters, ordered by decreasing OXPHOS score levels. (G) UMAP visualization of mature AMs categorized by relative *Crif1* expression levels. (H) OXPHOS module scores in *Crif1*-low and *Crif1*-high mature AMs. (I) RNA-seq analysis of mononuclear phagocytes from the ImmGen project showing normalized *Crif1* gene expression from individual TRM sample datasets (AM, n=7; microglia, n=19; Kupffer cell, n=7; PM, n=31; RPM, n=4). (J) Relative levels of mitochondrial ROS, membrane potential, and mass in TRMs, measured via flow cytometry (n=2–5). Mitochondrial ROS, membrane potential, and mass were assessed using MitoSOX Red, MitoTracker Orange, and MitoTracker Green staining, respectively. Fold changes in MFI compared to AM were calculated for each cell type. (K) CRIF1 expression levels in TRMs, measured via flow cytometry (n=4–6). Representative plots are shown. Dots represent individual samples or mice.
MFI, mean fluorescence intensity.
The p-values are presented as follows: *p<0.05, **p<0.01, ***p<0.001, and ****p<0.0001.


https://doi.org/10.4110/in.2025.25.e9

Macrophages exhibit differential metabolic preferences based on their tissue microenvironment (3). To characterize the metabolic preferences for mitochondria-mediated OXPHOS among TRMs, we examined the mitochondrial profiles of macrophages from the lung, brain, liver, peritoneum, and spleen in mice under steady state. Consistent with the AM-specific increase in expression levels of OXPHOS-related genes revealed by scRNA-seq analysis (**Fig. 1B**), mitochondrial ROS and MMP in AMs were greater than in microglia, Kupffer cells, PMs, and RPMs (**Fig. 1J**). Lung AMs also exhibited high mitochondrial mass, second to microglia and above all other TRM subsets. AMs showed higher mitochondrial ROS, MMP, and mass than hematopoietic stem cell-derived IMs (15) despite being under the same lung microenvironment (**Fig. 1J**). This suggests that AMs use more mitochondria as their metabolic source compared to other macrophages. Furthermore, the expression of mitochondrial regulator CRIF1 was also higher in AMs among several types of TRMs (**Fig. 1K**). Altogether, AMs were characterized by heightened mitochondrial parameters, along with pronounced expression levels of CRIF1.

## CRIF1 plays a critical role in the maintenance of AMs, but not other TRMs

To explore the role of CRIF1 in TRMs, we crossed LysM-Cre mice with *Crif1*-floxed mice to obtain LysM-Cre *Crif1*$^{fl/fl}$ (*Crif1*-mKO) mice, which lack CRIF1 in macrophages (**Supplementary Fig. 2A**). We confirmed successful deletion of CRIF1 in these mice at the transcriptional and translational levels (**Supplementary Fig. 2B and C**). The absence of CRIF1 did not impact BMDM generation (**Supplementary Fig. 2D**). However, *Crif1*-mKO BMDMs showed a higher ECAR and a lower OCR relative to control (LysM-Cre) BMDMs (**Supplementary Fig. 2E and F**). In addition, *Crif1*-mKO BMDMs demonstrated a reduction in mitochondrial mass (**Supplementary Fig. 2G**). These findings suggest that CRIF1 is not required for *in vitro* BMDM differentiation; however, CRIF1-deficient macrophages depend on anaerobic glycolysis because their ability to use the more efficient OXPHOS pathway is restricted.

Given the variable expression of CRIF1 across TRMs (**Fig. 1K**), we hypothesized that CRIF1 may differentially contribute to regulating metabolic fitness in macrophages from various organs. To this end, we assessed macrophage populations present in various organs in control and *Crif1*-mKO mice, and found drastic reduction of AMs in *Crif1*-mKO mice compared to control mice (**Fig. 2A**). Conversely, the numbers of TRMs in the brain, liver, peritoneum, and spleen were not altered significantly by the loss of CRIF1 (**Fig. 2A**). Although *Crif1*-mKO mice harbored very few AMs in the lung compared to controls, they retained equal numbers of IMs (**Fig. 2B**, **Supplementary Fig. 2H**). AMs patrol the alveolar airspace for clearance of apoptotic cells, pathogens, excess surfactant, and various airway particles (16). *Crif1*-mKO mice similarly exhibited a lower percentage of AMs in their BAL fluid compared to control mice (**Fig. 2C**, **Supplementary Fig. 2H**). In concordance with its elevated level of expression, CRIF1 was necessary for the maintenance of lung AMs.

Mature AMs express the receptor Siglec-F, a sialic acid-binding lectin. *Crif1*-mKO mice showed significantly reduced numbers of Siglec-F$^{+}$CD11b$^{-}$ mature AMs in the total lungs, while Siglec-F$^{-}$CD11b$^{+}$ immature AM-like cells (17) were not affected (**Fig. 2D**). A similar reduction in mature AMs was observed in BAL fluid from *Crif1*-mKO mice (**Fig. 2E**). The decline in AM proportions were more pronounced as mice were aged, from the point of weaning (4 wk) to a juvenile stage (6 wk), and to a mature adult stage (8 wk) (**Fig. 2F and G**). The nearly complete loss of mature AMs suggests that CRIF1 is critical for the integrity of these populations.


https://doi.org/10.4110/in.2025.25.e9

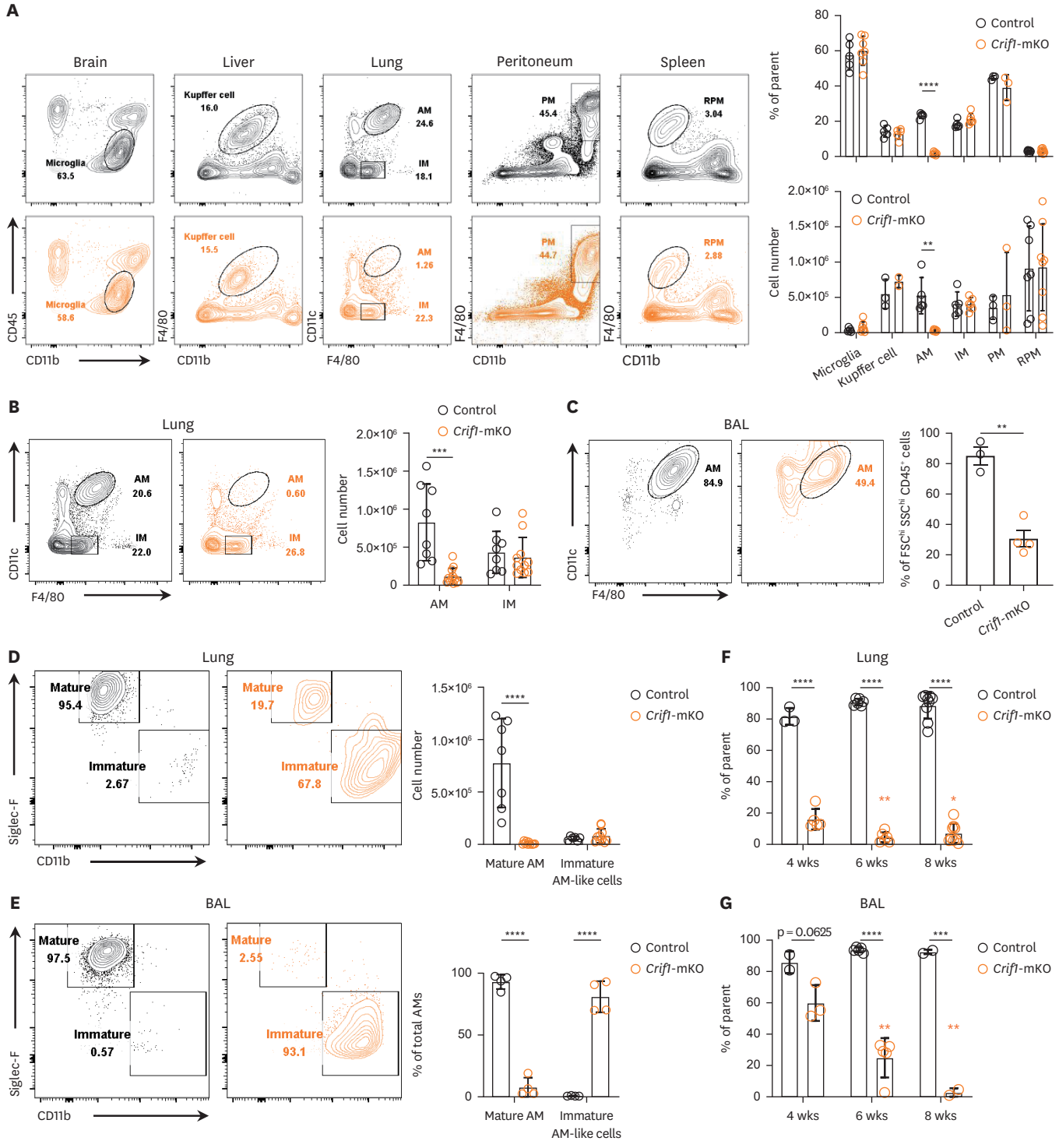


**Figure 2.** CRIF1 plays a critical role in the maintenance of AMs.
(A) Analysis of TRMs in the brain, liver, lung, peritoneal cavity, and spleen of control and *Crif1*-mKO mice. Proportions among singlet, live, CD45-positive, size-gated cells (n=3–8) and total cell counts (n=2–8) were evaluated. (B) Proportion and number of AMs and IMs in the lungs (n=8–12). (C) Proportion of BAL fluid AMs (n=3–4). (D) Proportion and number of mature AMs and immature AM-like cells in the lungs (n=7–11). (E) Proportion of mature AMs and immature AM-like cells in BAL fluid (n=4). (F and G) Maturation status of AMs in the lung (F; n=3–9) and BAL fluid (G; n=2–5) from 4 to 8 wk of age, measured by the proportion of Siglec-F$^+$CD11b$^-$ mature AMs among total AMs. Representative plots are shown. Dots represent individual mice.
The p-values are presented as follows: **p<0.01, ***p<0.001, and ****p<0.0001.


https://doi.org/10.4110/in.2025.25.e9

## CRIF1 regulates mitochondrial function and lipid turnover in AMs

Next, to investigate the mechanisms by which CRIF1 regulates the development and maintenance of AMs, we explored the mitochondrial phenotypes and metabolic characteristics of AMs in *Crif1*-mKO mice. Mitochondrial biogenesis is a process by which cells increase the number of or expand the size of mitochondria. In response to various external stress signals such as nutrient deprivation, oxidative stress, DNA damage, and ER stress, cells reconstruct their metabolic state, with mitochondrial biogenesis being a major adaptation method (18). Thus, the evaluation of mitochondrial mass has been used as an indicator of mitochondrial biogenesis since changes in biogenesis are reflected by changes in mitochondrial mass (19-21). CRIF1-deficient AMs exhibited decreased mitochondrial mass, as measured by MitoTracker Green staining (**Fig. 3A**). Other parameters of mitochondrial function, including mitochondrial ROS and MMP, were also measured using MitoSOX Red and MitoTracker Orange staining, respectively. CRIF1-deficient AMs showed a modest decline in mitochondrial ROS, reflecting a reduction in electron transport chain activity, while MMP was not significantly altered (**Fig. 3A**). Given that ROS can activate mitobiogenesis regulators PGC-1α and NRF1 to enhance the expression of mitochondrial genes and antioxidant pathways (22,23), the interplay between ROS levels and mitochondrial biogenesis represents a tightly co-regulated and interdependent process. The loss of mitochondrial mass in mature AMs and the decreased ROS production in immature AMs in *Crif1*-mKO mice suggest significant mitochondrial alterations across different stages of AM development.

Furthermore, we measured the expression levels of MT-CO1 and SDHA in CRIF1-deficient AMs. MT-CO1 is a mitochondrial DNA-encoded OXPHOS complex IV subunit, and SDHA is a nuclear DNA-encoded OXPHOS complex II subunit. The ratio between these 2 mitochondrial proteins, which originate from different genomes, represents relative mitochondrial translation. Interestingly, the MT-CO1 to SDHA ratio was decreased in CRIF1-deficient mature AMs (**Fig. 3B**), indicating dysregulated mitochondrial protein synthesis in CRIF1-deficient AMs. These findings collectively support that that CRIF1 is essential for maintaining normal mitochondrial function.

Contrary to these mitochondrial functional defects, CRIF1-deficient AMs showed higher expression of the glucose transporter GLUT1, suggesting enhanced glucose metabolism (**Fig. 3C**). ATP levels were not reduced in CRIF1-deficient AMs compared to control AMs, indicating that glycolysis could compensate for energy production and suggesting that their reduction is not due to energy deficiency (**Fig. 3D**). A hallmark function of AMs is to promote lipid homeostasis in the lung by uptake and processing of excess surfactant (16). Intracellular lipid content was also higher in CRIF1-deficient AMs, suggesting that CRIF1 is required for lipid processing (**Fig. 3E**). Possibly reflecting these metabolic changes, *Crif1*-mKO AMs displayed an enlarged cytoplasm with increased number of vacuoles when visualized with Diff-Quik staining (**Fig. 3F**). Such lipid-laden macrophages, or foam cells, are observed in conditions such as pulmonary alveolar proteinosis (24). Consistently, side-scatter (SSC) measurements, which represent cell granularity, were also increased in CRIF1-deficient AMs (**Fig. 3G**).

To further explore the metabolic pathways and cellular functions regulated by CRIF1 expression, we conducted GSEA (9) on *Crif1*-high and *Crif1*-low AMs from our scRNA-seq analysis (**Fig. 1G**). As expected, *Crif1*-high AMs showed significant enrichment in gene sets related to OXPHOS and other mitochondrial functions (**Fig. 3H**, **Supplementary Fig. 3A and B**). Additionally, we found enrichment in gene sets involved in cholesterol homeostasis,

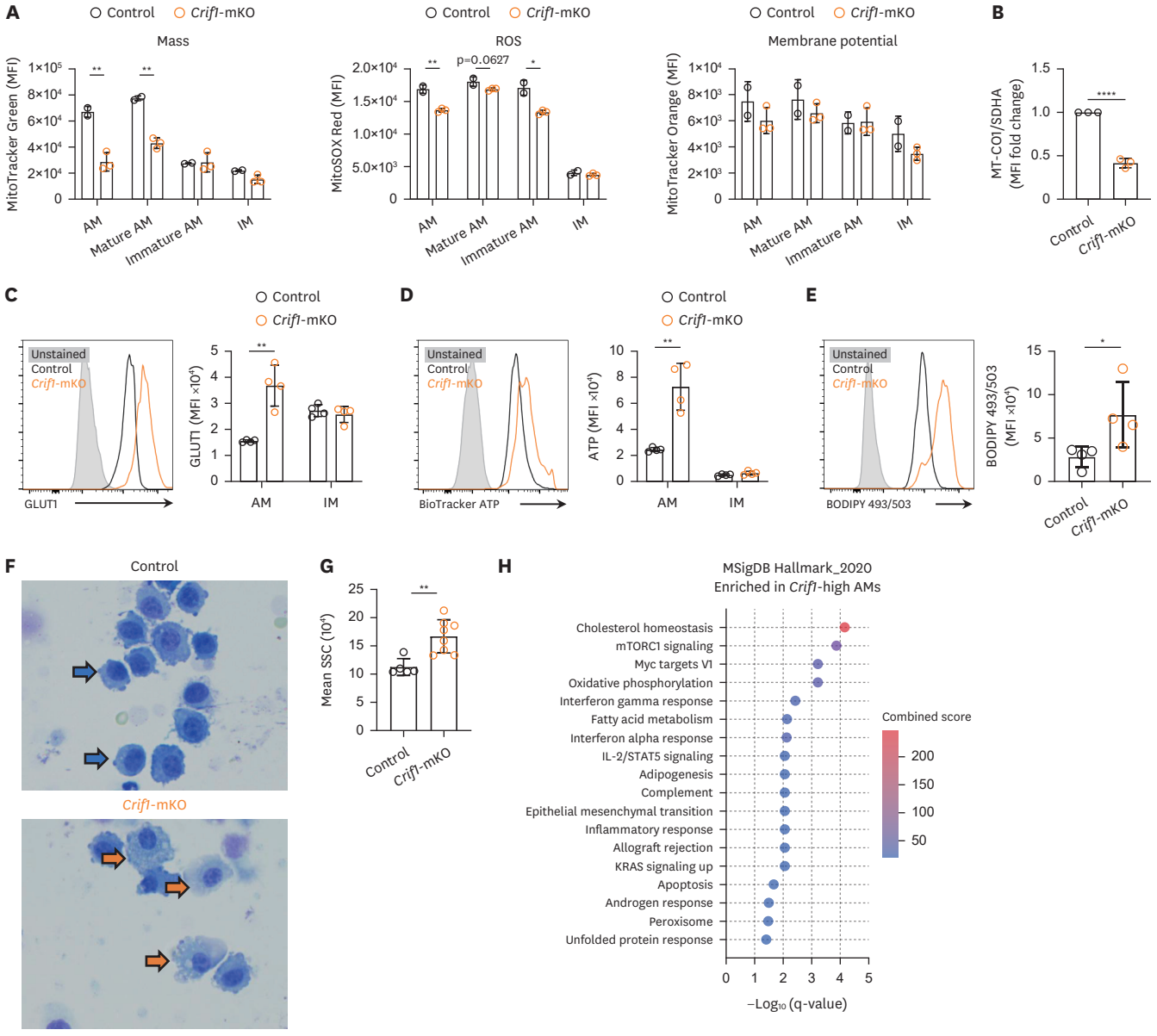


**Figure 3.** CRIF1-deficient AMs exhibit impaired mitochondrial function and lipid turnover.
(A) Mitochondrial mass, ROS, and membrane potential in lung macrophages in control and *Crif1*-mKO mice were measured via flow cytometry (n=2–3). Mitochondrial mass, ROS, and membrane potential were assessed by staining with MitoTracker Green, MitoSOX Red, and MitoTracker Orange, respectively. (B) Mitochondrial biogenesis rate, estimated by the ratio of MT-CO1 and SDHA expression was measured in mature AMs via flow cytometry (n=3). (C) GLUT1 expression in AMs and IMs (n=4). (D) ATP levels in AMs and IMs were quantified using BioTracker ATP (n=4). (E) Cellular neutral lipid content was quantified in mature AMs by BODIPY 493/503 staining and flow cytometry (n=4). (F) BAL fluid from control and *Crif1*-mKO mice was stained with Diff-Quik and morphologies of AMs were visualized under a light microscope (n=3). (G) SSC of AMs were measured and quantified via flow cytometry (n=5–8). (H) scRNA-seq data analysis of *Crif1*-high and *Crif1*-low mature AMs. GSEA using the Hallmark_2020 library performed with the EnrichR package. Pathways that were significantly enriched in *Crif1*-high AMs with an adjusted p-value (q-value) <0.05 are listed. Representative plots are shown. Dots represent individual mice.
SSC, side-scatter; MFI, mean fluorescence intensity.
The p-values are presented as follows: *p<0.05, **p<0.01, and ****p<0.0001.

fatty acid metabolism, and adipogenesis, which aligned with the accumulation of neutral lipids observed in the AMs of *Crif1*-mKO mice (**Fig. 3E and H**). Interestingly, beyond these metabolism-related pathways, *Crif1*-high AMs also exhibited enrichment in various immune response regulatory pathways, as well as mTOR complex 1 signaling, epithelial-mesenchymal transition, apoptosis, protein catabolism, Ag processing and presentation, and phagocytosis


https://doi.org/10.4110/in.2025.25.e9

(**Fig. 3H**, **Supplementary Fig. 3A**). These findings suggest that CRIF1-mediated regulation of mitochondrial function may influence not only energy metabolism but also impact key functional properties of AMs.

Altogether, our results highlight the multifaceted role of CRIF1 in maintaining metabolic processes and the functionality of AMs.

## DISCUSSION

In this study, we identified CRIF1 as a critical regulator of mitochondrial function and metabolic fitness specifically in AMs. CRIF1 is required for AM maintenance, as its deletion led to a selective loss of AM populations in the lung, while other TRMs remained unaffected. In contrast, TFAM KO mice harbor a reduced number of TRMs in the lung, liver, peritoneum, spleen, and skin (4). These findings highlight the specific role of CRIF1 in the maintenance of AMs, in contrast to the effects of TFAM on a broad range of TRMs across multiple organs. Unlike TFAM, CRIF1 might specialize in regulating mitochondrial homeostasis in AMs, but not other organ TRMs. This distinction underscores the need to explore tissue-specific regulators like CRIF1, which may operate within specific immune environments.

The metabolic reprogramming observed in CRIF1-deficient AMs, characterized by increased glycolysis, loss of OXPHOS, and aberrant lipid accumulation, may be attributed to a significant adaptation to mitochondrial dysfunction. However, CRIF1-deficient AMs did not show signs of energy depletion. The exact mechanisms by which CRIF1-mediated mitochondrial insufficiency in AMs leads to abnormal lipid accumulation are not fully understood. It is potentially possible that the impairment of mitochondrial fatty acid oxidation might be crucial for the clearance of excess lipids, resulting in lipid accumulation in CRIF1-deficient AMs. This is further supported by significant enrichment of fatty acid metabolism in *Crif1*-high AMs in enrichment analysis. Mitochondrial dysfunction has been reported to cause Golgi apparatus disorganization and disrupt lipid transport within the secretory pathway (25). Furthermore, peroxisome proliferator-activated receptor-γ (PPAR-γ), a master regulator for adipogenesis, is a critical transcription factor for AM development (26). Chromatin immunoprecipitation sequencing data indicate that PPAR-γ may act as an upstream transcriptional regulator of CRIF1 (27). However, PPAR-γ is also highly expressed in RPMs (26,28), yet RPMs do not express CRIF1 at levels comparable to AMs, nor is their development affected by CRIF1 deletion. Along with PPAR-γ, additional co-regulatory factors or microenvironmental cues likely influence CRIF1 expression and function in AMs. Furthermore, as OXPHOS functionality is particularly critical for AMs among TRMs (4), the differential dependence on mitochondrial function may explain the significance of CRIF1 in AMs. Thus, further studies on the tissue-specific CRIF1-mediated regulation of gene expression in AMs could provide valuable insights into the mechanisms underlying mitochondrial function and lipid homeostasis in these cells.

The role of CRIF1 in regulating mitochondrial function extends beyond energy metabolism to influence key immune functions in AMs. Enrichment analysis uncovered that *Crif1*-high AMs exhibited enrichment of gene expression involved in OXPHOS and fatty acid metabolism, but also in immune pathways such as cytokine responses, Ag processing and Ag presentation. These findings suggest that CRIF1 may coordinate mitochondrial functions with other essential immune functions in AMs.

In conclusion, our study revealed that CRIF1 is an essential regulator of mitochondrial function, metabolic homeostasis, and the maintenance of AMs. These results provide new insights into CRIF1-dependent, tissue-specific regulation of AMs, which is distinct from mitochondrial programs globally regulated by TFAM in TRMs. Thus, these findings shed light on the potential role of CRIF1 as a therapeutic target for conditions involving AM dysfunction.

## ACKNOWLEDGEMENTS

This research was supported by a grant of the MD-PhD/Medical Scientist Training Program through the Korea Health Industry Development Institute (KHIDI), funded by the Ministry of Health & Welfare, Republic of Korea. This research was also supported by Basic Science Research Program through the National Research Foundation of Korea (NRF) funded by the Ministry of Science and ICT (RS-2023-00217571 and RS-2020-NR048827). We would like to appreciate technical assistance by Yeon Duk Woo.

## SUPPLEMENTARY MATERIALS

### Supplementary Figure 1

Transcriptomic analyses of mitochondrial phenotypes in various TRMs.

### Supplementary Figure 2

Generation of *Crif1*-mKO mice.

### Supplementary Figure 3

Enrichment analysis of *Crif1*-high and low AMs.

## REFERENCES

1. Mass E, Nimmerjahn F, Kierdorf K, Schlitzer A. Tissue-specific macrophages: how they develop and choreograph tissue biology. *Nat Rev Immunol* 2023;23:563-579. PUBMED | CROSSREF
2. Russell DG, Huang L, VanderVen BC. Immunometabolism at the interface between macrophages and pathogens. *Nat Rev Immunol* 2019;19:291-304. PUBMED | CROSSREF
3. Wculek SK, Dunphy G, Heras-Murillo I, Mastrangelo A, Sancho D. Metabolism of tissue macrophages in homeostasis and pathology. *Cell Mol Immunol* 2022;19:384-408. PUBMED | CROSSREF
4. Wculek SK, Heras-Murillo I, Mastrangelo A, Mañanes D, Galán M, Miguel V, Curtabbi A, Barbas C, Chandel NS, Enríquez JA, et al. Oxidative phosphorylation selectively orchestrates tissue macrophage homeostasis. *Immunity* 2023;56:516-530.e9. PUBMED | CROSSREF
5. O'Neill LAJ, Pearce EJ. Immunometabolism governs dendritic cell and macrophage function. *J Exp Med* 2016;213:15-23. PUBMED | CROSSREF
6. Gao X, Zhu B, Wu Y, Li C, Zhou X, Tang J, Sun J. TFAM-dependent mitochondrial metabolism is required for alveolar macrophage maintenance and homeostasis. *J Immunol* 2022;208:1456-1466. PUBMED | CROSSREF
7. Dick SA, Wong A, Hamidzada H, Nejat S, Nechanitzky R, Vohra S, Mueller B, Zaman R, Kantores C, Aronoff L, et al. Three tissue resident macrophage subsets coexist across organs with conserved origins and life cycles. *Sci Immunol* 2022;7:eabf7777. PUBMED | CROSSREF
8. Hao Y, Hao S, Andersen-Nissen E, Mauck WM 3rd, Zheng S, Butler A, Lee MJ, Wilk AJ, Darby C, Zager M, et al. Integrated analysis of multimodal single-cell data. *Cell* 2021;184:3573-3587.e29. PUBMED | CROSSREF

9. Xie Z, Bailey A, Kuleshov MV, Clarke DJB, Evangelista JE, Jenkins SL, Lachmann A, Wojciechowicz ML, Kropiwnicki E, Jagodnik KM, et al. Gene set knowledge discovery with Enrichr. *Curr Protoc* 2021;1:e90. PUBMED | CROSSREF
10. ImmGen Consortium. Open-source ImmGen: mononuclear phagocytes. *Nat Immunol* 2016;17:741. PUBMED | CROSSREF
11. Kwon MC, Koo BK, Moon JS, Kim YY, Park KC, Kim NS, Kwon MY, Kong MP, Yoon KJ, Im SK, et al. Crif1 is a novel transcriptional coactivator of STAT3. *EMBO J* 2008;27:642-653. PUBMED | CROSSREF
12. Lee S, Song SG, Kim G, Kim S, Yoo HJ, Koh J, Kim YJ, Tian J, Cho E, Choi YS, et al. CRIF1 deficiency induces FOXP3$^{LOW}$ inflammatory non-suppressive regulatory T cells, thereby promoting antitumor immunity. *Sci Adv* 2024;10:eadj9600. PUBMED | CROSSREF
13. Kim SJ, Kwon MC, Ryu MJ, Chung HK, Tadi S, Kim YK, Kim JM, Lee SH, Park JH, Kweon GR, et al. CRIF1 is essential for the synthesis and insertion of oxidative phosphorylation polypeptides in the mammalian mitochondrial membrane. *Cell Metab* 2012;16:274-283. PUBMED | CROSSREF
14. Jung SB, Choi MJ, Ryu D, Yi HS, Lee SE, Chang JY, Chung HK, Kim YK, Kang SG, Lee JH, et al. Reduced oxidative capacity in macrophages results in systemic insulin resistance. *Nat Commun* 2018;9:1551. PUBMED | CROSSREF
15. Bedoret D, Wallemacq H, Marichal T, Desmet C, Quesada Calvo F, Henry E, Closset R, Dewals B, Thielen C, Gustin P, et al. Lung interstitial macrophages alter dendritic cell functions to prevent airway allergy in mice. *J Clin Invest* 2009;119:3723-3738. PUBMED | CROSSREF
16. Aegerter H, Lambrecht BN, Jakubzick CV. Biology of lung macrophages in health and disease. *Immunity* 2022;55:1564-1580. PUBMED | CROSSREF
17. Woo YD, Koh J, Ko JS, Kim S, Jung KC, Jeon YK, Kim HY, Lee H, Lee CW, Chung DH. Ssu72 regulates alveolar macrophage development and allergic airway inflammation by fine-tuning of GM-CSF receptor signaling. *J Allergy Clin Immunol* 2021;147:1242-1260. PUBMED | CROSSREF
18. Jornayvaz FR, Shulman GI. Regulation of mitochondrial biogenesis. *Essays Biochem* 2010;47:69-84. PUBMED | CROSSREF
19. Davinelli S, Sapere N, Visentin M, Zella D, Scapagnini G. Enhancement of mitochondrial biogenesis with polyphenols: combined effects of resveratrol and equol in human endothelial cells. *Immun Ageing* 2013;10:28. PUBMED | CROSSREF
20. Hwang JH, Kim KM, Oh HT, Yoo GD, Jeong MG, Lee H, Park J, Jeong K, Kim YK, Ko YG, et al. TAZ links exercise to mitochondrial biogenesis via mitochondrial transcription factor A. *Nat Commun* 2022;13:653. PUBMED | CROSSREF
21. Li S, Li W, Yuan J, Bullova P, Wu J, Zhang X, Liu Y, Plescher M, Rodriguez J, Bedoya-Reina OC, et al. Impaired oxygen-sensitive regulation of mitochondrial biogenesis within the von Hippel-Lindau syndrome. *Nat Metab* 2022;4:739-758. PUBMED | CROSSREF
22. Suzuki H, Kumagai T, Goto A, Sugiura T. Increase in intracellular hydrogen peroxide and upregulation of a nuclear respiratory gene evoked by impairment of mitochondrial electron transfer in human cells. *Biochem Biophys Res Commun* 1998;249:542-545. PUBMED | CROSSREF
23. St-Pierre J, Drori S, Uldry M, Silvaggi JM, Rhee J, Jäger S, Handschin C, Zheng K, Lin J, Yang W, et al. Suppression of reactive oxygen species and neurodegeneration by the PGC-1 transcriptional coactivators. *Cell* 2006;127:397-408. PUBMED | CROSSREF
24. Trapnell BC, Nakata K, Bonella F, Campo I, Griese M, Hamilton J, Wang T, Morgan C, Cottin V, McCarthy C. Pulmonary alveolar proteinosis. *Nat Rev Dis Primers* 2019;5:16. PUBMED | CROSSREF
25. Moschandrea C, Kondylis V, Evangelakos I, Herholz M, Schneider F, Schmidt C, Yang M, Ehret S, Heine M, Jaeckstein MY, et al. Mitochondrial dysfunction abrogates dietary lipid processing in enterocytes. *Nature* 2024;625:385-392. PUBMED | CROSSREF
26. Schneider C, Nobs SP, Kurrer M, Rehrauer H, Thiele C, Kopf M. Induction of the nuclear receptor PPAR-γ by the cytokine GM-CSF is critical for the differentiation of fetal monocytes into alveolar macrophages. *Nat Immunol* 2014;15:1026-1037. PUBMED | CROSSREF
27. Menéndez-Gutiérrez MP, Rőszer T, Fuentes L, Núñez V, Escolano A, Redondo JM, De Clerck N, Metzger D, Valledor AF, Ricote M. Retinoid X receptors orchestrate osteoclast differentiation and postnatal bone remodeling. *J Clin Invest* 2015;125:809-823. PUBMED | CROSSREF
28. Gautier EL, Chow A, Spanbroek R, Marcelin G, Greter M, Jakubzick C, Bogunovic M, Leboeuf M, van Rooijen N, Habenicht AJ, et al. Systemic analysis of PPARγ in mouse macrophage populations reveals marked diversity in expression with critical roles in resolution of inflammation and airway immunity. *J Immunol* 2012;189:2614-2624. PUBMED | CROSSREF